

High-speed scalability of synchronous reluctance machines considering different lamination materials

Original

High-speed scalability of synchronous reluctance machines considering different lamination materials / Palmieri, M.; Perta, M.; Cupertino, F.; Pellegrino, GIAN - MARIO LUIGI. - STAMPA. - (2014), pp. 614-620. (40th Annual Conference of the IEEE Industrial Electronics Society, IECON 2014 Sheraton Hotel Dallas, usa 2014)
[10.1109/IECON.2014.7048564].

Availability:

This version is available at: 11583/2634090 since: 2016-02-21T11:55:43Z

Publisher:

Institute of Electrical and Electronics Engineers Inc.

Published

DOI:10.1109/IECON.2014.7048564

Terms of use:

This article is made available under terms and conditions as specified in the corresponding bibliographic description in the repository

Publisher copyright

IEEE postprint/Author's Accepted Manuscript

©2014 IEEE. Personal use of this material is permitted. Permission from IEEE must be obtained for all other uses, in any current or future media, including reprinting/republishing this material for advertising or promotional purposes, creating new collecting works, for resale or lists, or reuse of any copyrighted component of this work in other works.

(Article begins on next page)

High-Speed Scalability of Synchronous Reluctance Machines Considering Different Lamination Materials

M. Palmieri, M. Perta, F. Cupertino
Department of Electrical Engineering
Politecnico di Bari
Bari, Italy
francesco.cupertino@poliba.it

G. Pellegrino
Department of Energy
Politecnico di Torino
Torino, Italy
gianmario.pellegrino@polito.it

Abstract—This paper considers the design of synchronous reluctance (SyR) machines for high-speed applications with the aid of optimization algorithms and considering both electromagnetic and mechanical performances. The design of small SyR machines with rated speeds from 5krpm to 50krpm is investigated, using two commercial laminations: a cobalt iron alloy and a high-grade non-oriented silicon steel. The integrity of the SyR rotors is guaranteed by the structural ribs and posts connecting the steel segments, so to simplify motor construction, without any retaining sleeves. The silicon steel, despite the lower magnetic performances respect to the cobalt iron, appears a competitive choice in high-speed applications due to its superior mechanical performances. Extensive design optimization, magnetic and structural finite element analysis demonstrate the feasibility of such high-speed SyR machines.

Keywords— *AC motors; Design automation; Pareto optimization; Synchronous reluctance machines; High-speed electrical machines.*

I. INTRODUCTION

High-speed electrical machines are gaining a growing interest in the recent years because they allow reducing weight and size and/or avoiding the use of mechanical gearboxes [1]. As a general rule, any brushless AC machine could be used in high-speed applications but a special care must be devoted to the robustness of the rotor structure [2-3]. Moreover, in aeronautical applications machine performances have to be guaranteed also in low-pressure environment. Then, the rotor cooling becomes a critical issue that could be faced using complicated shaft cooling systems and/or reducing rotor losses.

Very high rotational speeds, from 100,000 to 500,000 rpm, have been recently reached using surface permanent magnet (PM) motors using retaining sleeves to ensure rotor integrity [3-4]. A retaining sleeve has been also adopted for an 8kW 40,000 rpm internal permanent magnet (IPM) machine in [5]. Unfortunately, retaining sleeves increase losses and make rotor construction more complicated. Cage rotor and even more solid rotor induction machines have an inherently robust rotor structure that is suitable for high speed but is characterized by higher rotor losses and lower torque density with respect to PM machines [3]. Alternative solutions to avoid rotor sleeves could be also offered by solid rotor synchronous reluctance (SyR) machines [6-7], but special manufacturing processes and special

materials are needed to achieve satisfactory performances in terms of torque density and efficiency.

Low speed SyR motors are usually realized using non-oriented laminations cut so to obtain rotors with multiple flux barriers [8-9]. Such machines are easy to manufacture, use standard processes, have no PMs and their excitation field can be arbitrarily adjusted to limit iron losses at zero torque. Their use in high-speed applications without a retaining sleeve is usually discouraged because the thickness of structural ribs has to be increased to ensure rotor integrity, thus potentially compromising machine performances.

This paper compares the performances that can be obtained in a wide speed range using two different lamination materials: a cobalt-iron alloy with very high magnetic saturation level and a high-grade silicon steel with low losses and extremely high yield strength. The paper presents the design of several SyR machines with rated speed ranging from 5 krpm to 50 krpm. All the considered machines share the same rated torque and outer envelope. The machines are designed with the aid of optimization algorithms so to improve the electromagnetic performances (torque and torque ripple). The electromagnetic optimization also adapts the thickness of the structural ribs to the rated speed according to simplified analytical relationships. After the electromagnetic optimization the structural integrity of the rotor is FEA validated. At the end of the geometry optimization process, the efficiency and losses distributions of all the machines are calculated and compared. The results demonstrate that the advantages of the cobalt-iron progressively vanish with the increase of the speed rating, due to the increasing thicknesses of the structural ribs. From 25 krpm on the low loss, high strength silicon steel becomes the best candidate for high-speed SyR machine manufacturing.

II. PROBLEM STATEMENT

A. Key aspect of rotor structural ribs

The stator and rotor geometries are defined in Fig. 2. The 2 interior barriers of the rotor are angled and similar to the shape of a U, whereas the outer barrier is straight and I shaped, so hereafter it will be indicated with the acronym I2U. It is worth noticing that the thicker are the tangential and radial ribs the stronger is the rotor structure at high speed. Conversely, the presence of thick inter-segment bridges short-circuit the rotor insulation, thus increasing the flux linkage of the insulation of

the high reluctance q -axis with negative impact both on torque and power factor. As described in [10] the choice of the 12U rotor can help in this respect, because of the very compact shape of its iron segments, that results in a reduced peripheral mass and centrifugal force to be withstood by the structural bridges. Circular barriers in [10], for example, have a less advantageous tradeoff between magnetic and mechanical characteristics: for the same speed rating they require thicker bridges.

B. Motor specifications

The case study considered in this paper consists in the design of SyR machines having a target specifications of 1.6 Nm and 0.25 dm³ size limit for active parts. Several machines will be considered, having rated speed in the range 5 - 50 krpm and consequently rated power in the range 0.8 - 8 kW, because all the machines share the same rated torque. Table I reports the common machine specifications.

After a preliminary study, the outer stator diameter and the axial length of the stack were fixed to 80 mm and 50 mm respectively for all the considered machines. The airgap was set to 0.25 mm due to mechanical limitations. A cobalt-iron (CoFe) and a silicon-iron (SiFe) alloys with low losses for high speed applications were considered in order to evaluate their effect on machine performance in terms of total losses and losses distribution between copper and iron. The first grade is the CoFe alloy Vacodur49, produced by Vacuumschmelze [11] with a lamination thickness of 0.15 mm and two different annealing treatments:

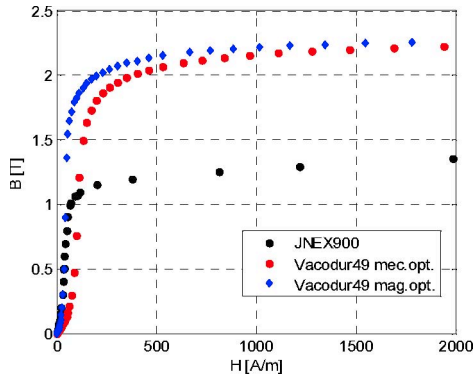


Fig. 1 - B-H characteristics of the considered lamination materials

TABLE I
MACHINE SPECIFICATIONS

Parameter	Value	Units
Rated speed	5000 : 50000	rpm
Rated torque	1.6	Nm
Torque ripple	< 10	%
Pole pairs	2	--
Stator slots	24	--
Current density	< 15	A/mm ²
Slot filling factor	> 0.4	--
Shaft diameter	> 8	mm
Stator outer diameter	80	mm
Axial length	50	mm

1. Vacodur49-mec-opt: ensures optimal mechanical properties (used for rotor)
2. Vacodur49-mag-opt: ensures optimal electromagnetic properties (used for stator)

Both Vacodur49 steels have a saturation magnetization greater than 2 T, while the yield strength is 390 MPa for the mechanically optimized lamination. The second grade is the SiFe alloy 10JNEX900 produced by JFE Steel Corporation [12] with a lamination thickness of 0.1 mm, a lower saturation magnetization (1.5 T) but improved mechanical behavior (yield strength around 600 MPa). Fig. 1 shows the B-H curve for the aforementioned alloys and Table II reports the main lamination properties.

Three different rotational speeds (5 - 25 - 50 krpm) were considered as rated speeds for the designed SyR machines. For each considered rated speed two machines were designed, one using CoFe and one with SiFe alloy. The main stator and rotor geometric parameters of each SyR machine were designed automatically via the joint use of a multi-objective optimization algorithm and finite element magnetic, thermal and structural analysis [10, 13].

C. Motor parameterization

The automatic construction of the stator and rotor laminations was embedded into the optimization procedure by means of the Matlab scripting feature of FEMM [14]. All the considered machines have 24 stator slots and three rotor flux barriers per pole. These numbers have been extensively recognized by the related literature as one of the good stator - rotor combinations in terms of average torque to torque ripple tradeoff [15-16]. The stator parameters designed by the optimization algorithm are: the tooth height l_t , the tooth width w_t and the machine split ratio SR , defined as the ratio between stator inner and outer diameters. The above mentioned parameters are defined in Fig. 2a. The rotor geometry is shown in Fig. 2b. The rotor parameters automatically designed are the barriers width (hc_i) and their angular displacement at the airgap ($\Delta\alpha_i$). The tangential iron ribs (the ones at the flux barriers ends) were designed at an initial stage, according to the speed rating of each machine example and a preliminary test campaign. The dimensions of such tangential ribs are never changed during the optimization procedure. Where needed, inner posts were automatically added during the optimization, as described in subsection II.E. The final machine designs were validated by means of static structural FEA.

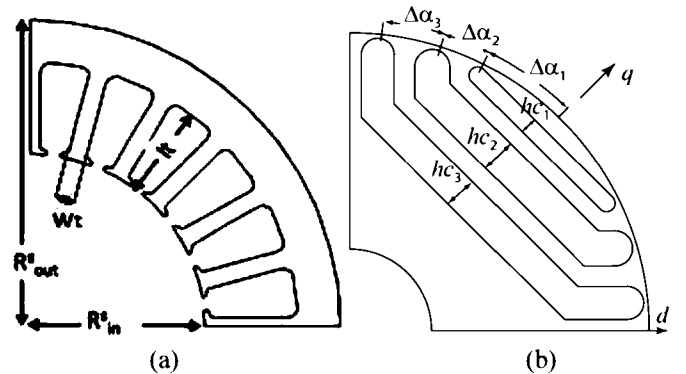


Fig. 2 – Parameterization of stator (a) and rotor (b) laminations.

TABLE II
ELECTRICAL AND MECHANICAL PROPERTIES OF THE IRON ALLOYS

Lamination Type	Vacodur opt-mec	Vacodur opt-mag	JNEX900
Loss \hat{a} 50 Hz, 1.5 T [W/kg]	2.78	1.27	1.46*
Loss \hat{a} 400 Hz, 1.5 T [W/kg]	26.4	14.7	14.8*
Yield strength [MPa]	390	210	604
Mass density [kg/m ³]	8120	8120	7490

* Extrapolated values

TABLE III
OPTIMIZATION PARAMETERS
AND LIMITS OF THE SEARCH SPACE

Parameter	Min value	Max value	Units
$hc_{1,2,3}$ (rotor)	0.2	1	p.u.
$\Delta\alpha_1$ (rotor)	16	27	degrees
$\Delta\alpha_{2,3}$ (rotor)	0.33	0.67	p.u.
SR (split ratio)	0.4	0.65	p.u.
l_t (stator)	10	14	mm
w_t (stator)	0.55	0.95	p.u.
γ (current angle)	50	70	degrees

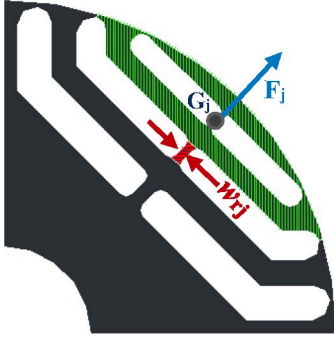


Fig. 3 – Definition of the inner posts geometry.

D. Torque per Ampere and Torque Ripple Optimization

The torque versus torque ripple optimization follows the guidelines described in [10, 13]. The phase angle γ of the current space vector is part of the set of optimization variables, so that each motor is evaluated very quickly in a single current angle condition. At the end of the torque ripple optimization, all the machines on the optimal Pareto front turn to be correctly evaluated in Maximum Torque per Ampere (MTPA) conditions, so to say that the optimization algorithm is capable to find the correct angle condition γ_{MTPA} maximizing the torque per Ampere and then the torque per copper loss.

The set of ten optimization parameters is summarized in Table III. The search bounds used in the paper are also reported. Where p.u. is indicated, it means that the value is in per-unit of the aggregate height or angle available for the layers or stator teeth.

E. Automatic Calculation of Radial Ribs thickness

The radial ribs thickness is calculated automatically for each barrier during the optimization process. The presence of tangential ribs is neglected in this stage. As shown in Fig. 3, the

j -th radial rib (red) supports the centrifugal stress of the green colored area. The corresponding mass M_j is then calculated:

$$M_j = \rho \cdot L \cdot \Sigma_j \quad (1)$$

where ρ is the mass density of the laminations, L is the machine axial length and Σ_j is the cross section of the part of lamination supported by the j -th barrier's rib (green area in Fig. 3). Secondly, the centrifugal force supported by the j -th radial rib is evaluated as if the mass M_j was concentrated in its center of gravity G_j :

$$F_j = M_j \cdot r_j \cdot \omega_{max}^2 \quad (2)$$

where r_j is the radius of the center of gravity and ω_{max} is the maximum rotational speed in rad/s. The polar coordinates of the considered center of gravity are $[r_j, \pi/(2n_p)]$.

Finally, the width w_{rj} of the j -th radial rib is calculated according to the lamination material Yield strength σ_{max} by (3):

$$w_{rj} = \frac{F_j}{(L \cdot K \cdot \sigma_{max})} \quad (3)$$

where $K \in [0.7, 1.0]$ is a safety factor.

The value w_{rj} is calculated at every new machine evaluation during the optimization: if its value is equal or greater than the minimum feasible thickness of the chosen cutting process then the radial rib is included into the corresponding layer, otherwise the radial rib is neglected and the tangential ribs are left alone against the centrifugal stress. This very simplified approach to the automatic design of structural ribs requires that all the final machines are re-evaluated via a static structural FEA, for validation against maximum stress and fatigue.

III. AUTOMATED DESIGN PROCEDURE

A. Optimization algorithm

There are many meta-heuristic algorithms for single- and multi-objective optimization problems. They have in common the use of a set of candidate solutions (population) that are iteratively modified according to some probabilistic rules and that converge to the global minimum of the objective function with a certain degree of probability. Multi-objective Differential Evolution (MODE) has been selected because it gave the best results in terms of time to converge and repeatability of the results [13].

B. High-Speed Machines Design

Hereinafter for sake of simplicity, each of the six optimized machines will be referred with an acronym containing a letter ("V" for Vacodur49 and "J" for 10JNEX900) and a number that indicates the rated speed expressed in krpm. For example, "V5" stands for a Vacodur49 lamination designed with a rated speed equal to 5 krpm.

The workflow of the automated design procedure consists of the following consecutive steps:

1. Machine geometry optimization: MODE optimization of torque per Ampere and torque ripple via fast magneto-static FEA simulations, using Matlab and FEMM [14].
2. Structural verification of the selected machines with Comsol Multiphysics.

3. Accurate evaluation of the machines performance: torque profile and iron losses calculation by means of transient FEA with MagNet by Infolytica [17]. The winding temperature and corresponding joule losses are evaluated with ThermNet by Infolytica.

For each of the 6 example cases (5, 25, 50 krpm, Vacodur and JNEX) the machine design optimization was repeated five times to have a redundancy of Pareto fronts and avoid local minima with short computational time. The first four runs (Global Search, GS) are executed with the search bounds reported in Table III. The best machine is selected out of the four Pareto fronts (GS machine). Then a local search (LS) refinement is executed with a fifth run using search bounds restricted to a $\pm 15\%$ variation with respect to the GS machine. Finally the LS machine is selected from the fifth Pareto front. The five Pareto fronts of the V50 case are reported in Fig. 4. This approach demonstrated to be more time effective than running single optimization runs of bigger size [13]. For each of the six cases, one machine was selected from the aggregated torque versus torque ripple Pareto fronts, as highlighted in Fig. 4.

The six final SyR machines were checked by means of structural FEA and then accurately re-evaluated with magnetic Transient with Motion FEA simulations. The re-evaluation with transient FEA is made of simulation with 180 rotor steps over one electrical period, repeated for different key current amplitude and phase combinations to characterize the machine comprehensively. Core loss are calculated according to the loss data provided by the manufacturers [11, 12, 17]. Finally, a thermal simulation was performed, to check that the copper temperature stays within the limit of insulation class H and to calculate the copper loss accordingly. Torque profiles, power factors, iron and copper losses distribution and efficiencies calculated in this post processing stage are shown next.

IV. RESULTS

Fig. 5 shows the optimized laminations obtained using Vacodur49 (left column) and 10JNEX900 (right column) at the different speed ratings.

A. Optimal Geometries

Tables IV and V report the main geometric parameters of the optimized machines. Some geometric parameters do not change a lot with the speed or the lamination material. This is the case of the α_i angles defining the positions of the flux barriers ends at the airgap.

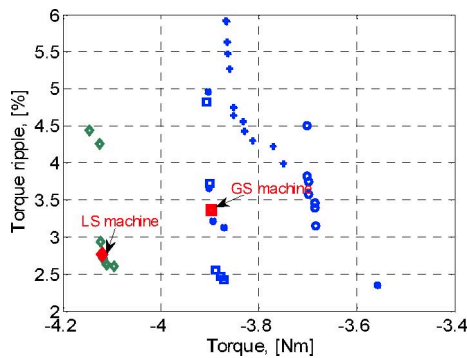


Fig. 4 – Pareto fronts obtained after five MODE runs.

This parameters have effect on the torque ripple because they determine the pitch of the equivalent rotor slots. All the optimized machines have equally-spaced rotor slots, in angular positions that match well with the ones that the literature would suggest for the considered 6 slots per pole stator [8]. The results in Tables IV and V confirm that torque ripple optimization has little to do with speed scaling.

Finally, there are parameters that depend on the specific material. All the SiFe machines have a ticker stator back-iron due to the reduced magnetic properties of the material. SiFe motors need smaller radial ribs to withstand centrifugal stresses due to high yield strength of 10JNEX900. This aspect become remarkable as speed increases because thinner ribs require low current to saturate, improving the machine performance in terms of average torque.

Fig. 6 shows the results of structural FEA analysis for V-series (left column) and J-series (right column) rotors with a 1:100 scale for the deformations. The colored scales are set according to the yield strength limit of the respective materials. In the radial ribs that have been designed during optimization, the stress approaches the Yield strength limit only at higher rotational speeds, as confirmed by the maximum stress values reported in tables VI and VII.

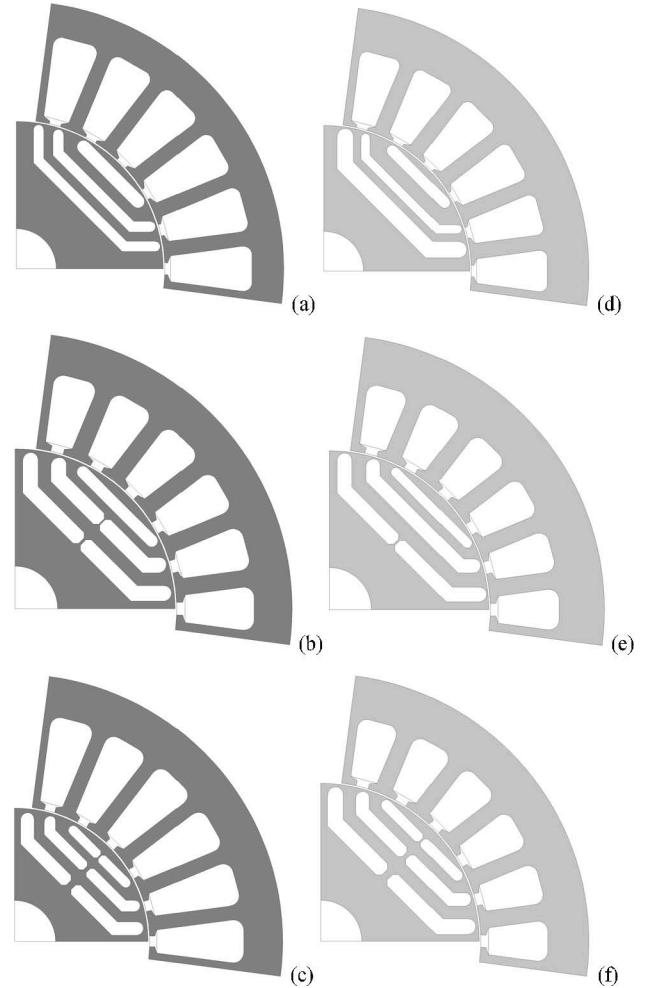


Fig. 5 – Machine laminations: V_5 (a), V_25 (b), V_50 (c), J_5 (d), J_25 (e), J_50 (f)

TABLE IV
VACODUR49 MACHINES – SELECTED MACHINES

Machine ID	V5	V25	V50
Split Ratio	0.55	0.58	0.50
Tangential rib (I-barrier) [mm]	0.20	0.20	0.20
Tangential rib (1 st U-barrier) [mm]	0.20	0.30	0.40
Tangential rib (2 nd U-barrier) [mm]	0.20	0.40	0.60
Radial rib (I-barrier) [mm]	-	-	0.32
Radial rib (1 st U-barrier) [mm]	-	0.21	0.99
Radial rib (2 nd U-barrier) [mm]	-	0.38	1.57
hc ₁ (I-barrier) [mm]	1.98	1.76	0.72
hc ₂ (1 st U-barrier) [mm]	1.60	2.19	1.70
hc ₃ (2 nd U-barrier) [mm]	1.55	2.23	2.32
α_1 [degree]	9	6	7
α_2 [degree]	18	17	17
α_3 [degree]	29	26	26
Tooth width [mm]	2.18	2.44	2.12
Tooth height [mm]	12.93	11.09	13.95

TABLE V
10JNEX900 MACHINES – SELECTED MACHINES

Machine ID	J5	J25	J50
Split Ratio	0.55	0.58	0.6
Tangential rib (I-barrier) [mm]	0.20	0.20	0.20
Tangential rib (1 st U-barrier) [mm]	0.20	0.20	0.30
Tangential rib (2 nd U-barrier) [mm]	0.20	0.20	0.40
Radial rib (I-barrier) [mm]	-	-	0.24
Radial rib (1 st U-barrier) [mm]	-	-	0.66
Radial rib (2 nd U-barrier) [mm]	-	0.26	1.10
hc ₁ (I-barrier) [mm]	1.71	1.45	1.65
hc ₂ (1 st U-barrier) [mm]	1.37	2.03	1.96
hc ₃ (2 nd U-barrier) [mm]	2.50	2.13	2.38
α_1 [degree]	9	6	6
α_2 [degree]	17	17	16
α_3 [degree]	29	26	26
Tooth width [mm]	2.33	2.45	2.50
Tooth height [mm]	11.48	10	10

TABLE VI
VACODUR MACHINES – MAXIMUM STRESS VALUES

Machine ID	V5	V25	V50	V50 _{mod}
Tangential ribs (I-barrier) [MPa]	16	368	280	300
Radial rib (I-barrier) [MPa]	-	-	210	255
Tangential ribs (1 st U-barrier) [MPa]	20	200	435	215
Radial rib (1 st U-barrier) [MPa]	-	70	240	408
Tangential ribs (2 nd U-barrier) [MPa]	28	200	400	210
Radial rib (2 nd U-barrier) [MPa]	-	130	280	305

TABLE VII
10JNEX900 MACHINES – MAXIMUM STRESS VALUES

Machine ID	J5	J25	J50	J50 _{mod}
Tangential ribs (I-barrier) [MPa]	16	415	340	540
Radial rib (I-barrier) [MPa]	-	-	210	340
Tangential ribs (1 st U-barrier) [MPa]	22	430	580	280
Radial rib (1 st U-barrier) [MPa]	-	-	350	430
Tangential ribs (2 nd U-barrier) [MPa]	25	455	610	280
Radial rib (2 nd U-barrier) [MPa]	-	130	340	500

B. Split of the Inner Post

The 50 krpm automatic designs have high stress levels in the tangential ribs, sometimes larger than the Yield strength limits of the respective materials. In such cases a possible, further mechanical optimization is suggested in Fig.7, where the inner posts are reshaped so to relax the stress level of the outer tangential ribs. The thick inner posts can be split into two separate posts having half width. These two are moved apart so to be closer to the tangential ribs. The split posts are also rotated in directions that converge when moving from the shaft to the airgap (see Fig. 7). Such inner ribs optimization was manually pursued and completed within a limited number of structural FEA iterations. The results of Fig. 7 show that the stress in the tangential ribs is well under the yield strength now. The electromagnetic performance of the two modified 50 krpm is unchanged because the total rib thickness was not changed during the structural refinement. The modified designs are referred to as V50_{mod} and J50_{mod} in tables VI and VII.

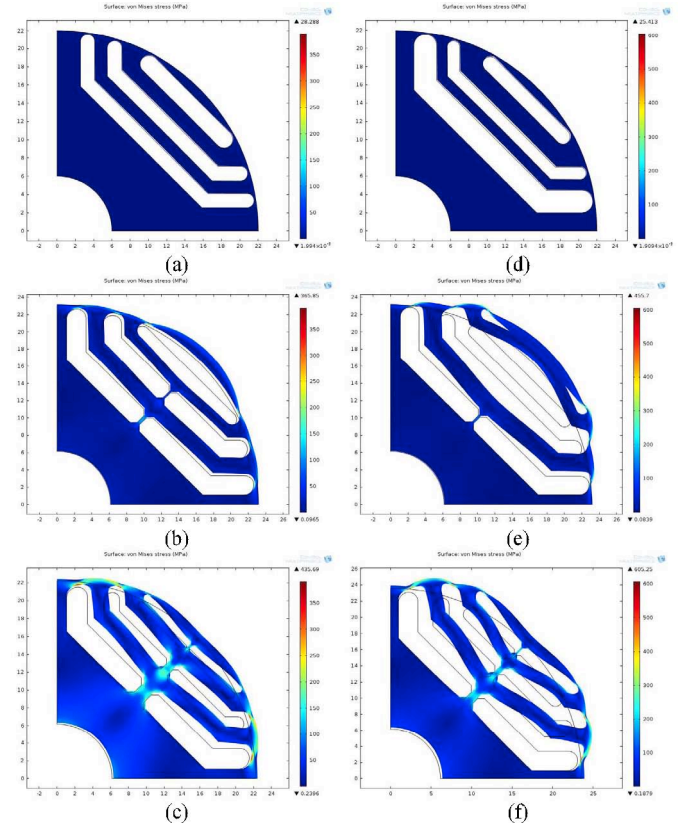


Fig. 6 – Structural FEA analysis: V5 (a), V25 (b), V50 (c), J5 (d), J25 (e), J50 (f)

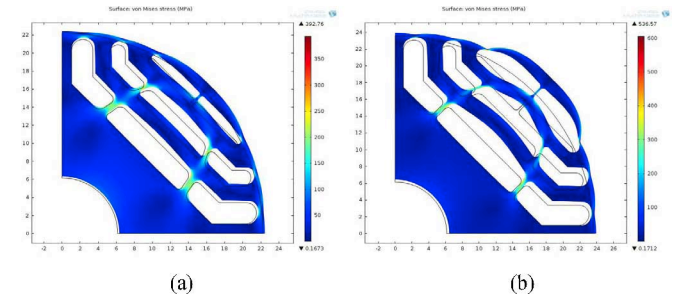


Fig. 7 – Structural FEA analysis of 50krpm with refined radial posts: V50_{mod} (a) and J50_{mod} (b).

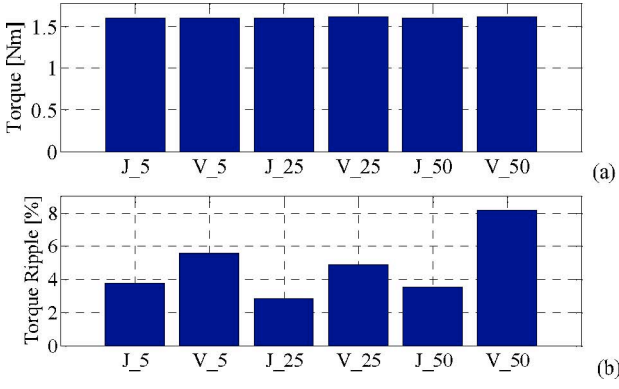


Fig. 8 – Average torque (a) and torque ripple (b)

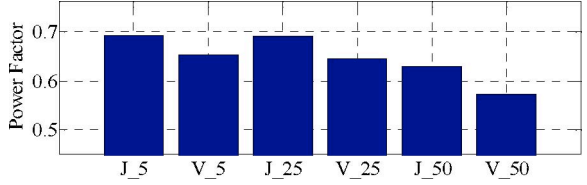


Fig. 9 – Power Factor

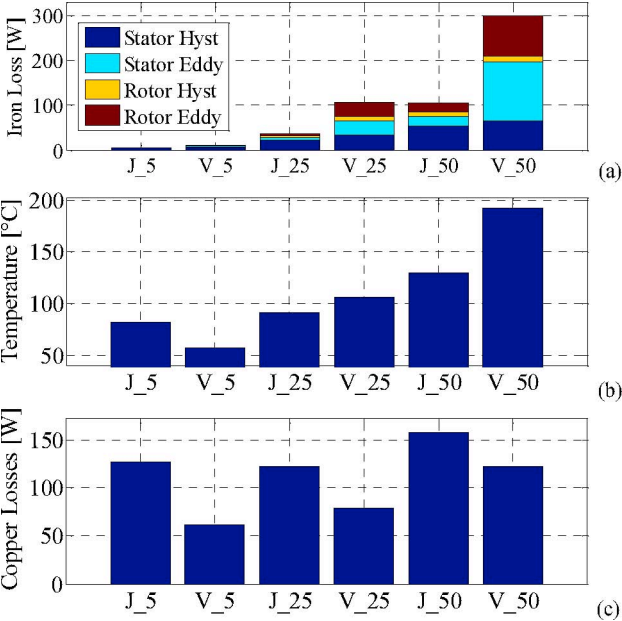


Fig. 10 – Iron losses (a) and copper temperature (b) and losses (c)

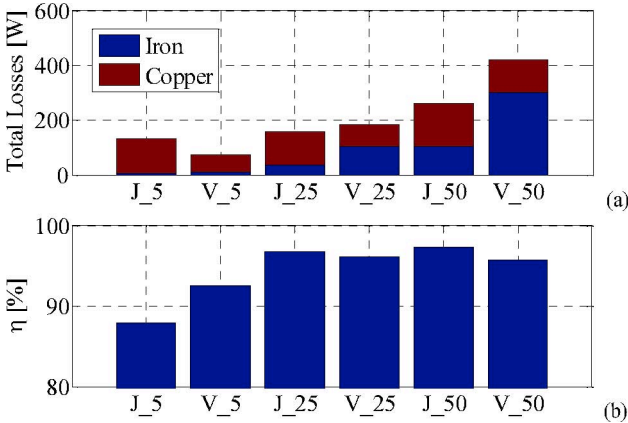


Fig. 11 – Total losses distribution (a) and efficiency (b)

C. Performance Figures

Fig. 8 shows the bar graphs of average torque and torque ripple for all the considered machines: torque ripple is evaluated as the standard deviation of torque over an exact number of periods. Both CoFe and SiFe motors fulfill the specifications listed in Table I: same torque $T = 1.6$ Nm, torque ripple lower than 10%. As the speed increases, the torque ripple slightly degrades but remains always lower for SiFe machines. Fig. 9 compares the power factor at same torque. As the speed increases, the power factor deteriorates due to the ticker structural ribs that leak larger quantities of q -flux linkage and reduce the machine saliency. The internal power factor (IPF), defined in (4), drops with the speed rating due to the decrease of the apparent saliency ratio L_d/L_q :

$$IPF = \frac{\frac{L_d}{L_q} - 1}{\frac{L_d}{L_q} + 1} \quad (4)$$

The J-series machines exhibit better PF values than V-series ones at all speeds. In fact, the adoption of a very high saturation iron such as CoFe alloys can produce disadvantages in this sense: the q -axis flux leaked by the saturated structural ribs is also much higher than the SiFe steel one, leading to lower power factor figures.

Fig. 10a shows iron losses distribution between hysteresis and eddy current for rotor and stator laminations, highlighting different behaviors for the two considered alloys. For every speed value, J-series machines exhibit lower iron losses than V-series. In SiFe laminations (J-), the stator loss dominates at every speed value and hysteresis losses are prevalent. Regarding the CoFe alloy (V-), the difference between stator and rotor iron losses is less pronounced. Moreover, eddy current losses have a major impact above 25 krpm in this case.

Fig. 11 reports the detail of iron and copper losses and overall efficiency. It is clear that at 5000 rpm the use of CoFe is advantageous in terms of efficiency, due to the higher torque per Joule loss density that can be achieved. All the J- machines require a greater current level to give the same target torque of the V-ones, due to the poorer magnetic properties of the SiFe material, resulting in higher copper losses and temperature for the same output power (Fig 10). At low speeds iron losses are negligible, so the efficiency of the V5-machine is higher than the one of the J5 competitor. Above 25 krpm this trend is reversed: for high rotational speeds, iron to copper losses ratio increases and then J-series motors become more efficient despite of the higher Joule loss. Plus, the J-machines maintain a more reasonable power factor.

V. CONCLUSION

This paper presented a comparative study of high-speed synchronous reluctance machines realized with two different lamination materials: a CoFe alloy and a high-grade SiFe alloy having worse magnetic characteristics but higher yield strength and lower losses. Several SyR machines have been designed by means of optimization algorithms coupled to FEA magnetic and structural analysis. The inclusion of the structural ribs size among the optimized parameters is one of the contributions of this work. The study has been applied to SyR machines having no retaining sleeves on the rotor: only tangential and radial ribs

guarantee rotor integrity. Such particular class of machines could be attractive in high-speed applications due to the simple construction. This study demonstrated that, above a certain speed, SiFe alloy guarantees better performances in terms of overall efficiency despite the lower magnetic performances of the material. We are currently working on the extension of this study to PM assisted SyR machines and on the inclusion of thermal analysis in the design optimization.

ACKNOWLEDGMENT

The Authors would like to thank Dario Bucci for his help in the realization of thermal finite element simulations. This work was supported in part by project PON MALET code PON01_01693.

REFERENCES

- [1] D. Gerada, A. Mebarki, N.L. Brown, C. Gerada, A. Cavagnino, A. Boglietti, "High-Speed Electrical Machines: Technologies, Trends, and Developments", *IEEE Transactions on Industrial Electronics*, Vol. 61, n. 6, 2014, pp. 2946-2959.
- [2] Hofmann H., Sanders S.R., "High-speed synchronous reluctance machine with minimized rotor losses", *IEEE Transactions on Industry Applications*, Vol. 36, n. 2, 2000, pp. 531-539.
- [3] Gerada D., Borg-Bartolo D., Mebarki A., Micallef C., Brown N.L., Gerada C., "Electrical machines for high speed applications with a wide constant-power region requirement", *International Conference on Electrical Machines and Systems, ICEMS 2011*.
- [4] Krahenbuhl D., Zwyssig C., Weser H., Kolar J.W., "A Miniature 500 000-r/min Electrically Driven Turbocompressor", *IEEE Transactions on Industry Applications*, Vol. 46, n. 6, 2010, pp. 2459-2466.
- [5] Sung-Il Kim, Young-Kyoun Kim, Geun-Ho Lee, Jung-Pyo Hong, "A Novel Rotor Configuration and Experimental Verification of Interior PM Synchronous Motor for High-Speed Applications", *IEEE Transactions on Magnetics*, Vol. 48, n. 2, 2012, pp. 843-846.
- [6] Jae-Do Park, Kalev C., Hofmann H.F., "Analysis and Reduction of Time Harmonic Rotor Loss in Solid-Rotor Synchronous Reluctance Drive", *IEEE Transactions on Power Electronics*, Vol. 23, n. 2, 2008, pp. 985-992.
- [7] Ikaheimo J., Kolehmainen J., Kansakangas T., Kivela V., Moghaddam R.R., "Synchronous High-Speed Reluctance Machine With Novel Rotor Construction", *IEEE Transactions on Industrial Electronics*, Vol. 61, n. 6, 2014, pp. 2969-2975.
- [8] Vagati, Alfredo, "Synchronous reluctance electrical motor having a low torque-ripple design," U.S. Patent No. 5,818,140, 6 Oct. 1998.
- [9] RR Moghaddam, "Rotor for a Synchronous Reluctance Machine", US Patent App. 13/230,543, 2011.
- [10] Pellegrino G., Cupertino F., Gerada C., "Barriers shapes and minimum set of rotor parameters in the automated design of Synchronous Reluctance machines" *IEEE International Electric Machines & Drives Conference (IEMDC)*, pp. 1204-1210, 2013.
- [11] <http://www.vacuumschmelze.com/>
- [12] <http://www.jfe-steel.co.jp/>
- [13] F. Cupertino, G. Pellegrino, C. Gerada, "Design of Synchronous Reluctance Machines with Multi-Objective Optimization Algorithms", *IEEE Transactions on Industry Applications*, DOI: 10.1109/TIA.2014.2312540, in press.
- [14] David Meeker, "Finite Element Method Magnetics", Ver. 4.2 User's Manual, February 5, 2009, [Online] available: <http://www.femm.info/Archives/doc/manual.pdf>
- [15] Vagati, A.; Pastorelli, M.; Francheschini, G.; Petrache, S.C., "Design of low-torque-ripple synchronous reluctance motors," *Industry Applications, IEEE Transactions on*, vol.34, no.4, pp.758-765, Jul/Aug 1998.
- [16] M. Palmieri, M. Perta, F. Cupertino, G. Pellegrino, "Effect of the numbers of slots and barriers on the optimal design of synchronous reluctance machines", *International Conference on Optimization of Electrical and Electronic Equipment, OPTIM 2014*
- [17] Infolytica MagNet: Design and analysis software for electromagnetics, [Online] available: www.infolytica.com